PCCP

Dynamic Article Links

Cite this: *Phys. Chem. Chem. Phys.*, 2012, **14**, 2434–2442

www.rsc.org/pccp

PAPER

The role of the Auger parameter in XPS studies of nickel metal, halides and oxides

Mark C. Biesinger,*[ab] Leo W. M. Lau,†[a] Andrea R. Gerson[b] and Roger St. C. Smart[b]

Received 26th July 2011, Accepted 14th December 2011
DOI: 10.1039/c2cp22419d

The critical role of the Auger parameter in providing insight into both initial state and final state factors affecting measured XPS binding energies is illustrated by analysis of Ni $2p_{3/2}$ and $L_3M_{45}M_{45}$ peaks as well as the Auger parameters of nickel alloys, halides, oxide, hydroxide and oxy-hydroxide. Analyses of the metal and alloys are consistent with other works, showing that final state relaxation shifts, ΔR, are determined predominantly by changes in the d electron population and are insensitive to inter-atomic charge transfer. The nickel halide Auger parameters are dominated by initial state effects, $\Delta\varepsilon$, with increasing positive charge on the core nickel ion induced by increasing electronegativity of the ligands. This effect is much greater than the final state shifts; however, the degree of covalency is reflected in the Wagner plot where the more polarizable iodide and bromide have greater ΔR. The initial state shift for NiO is much smaller than those of $Ni(OH)_2$ or NiOOH and the effective oxidation state is much less than that inferred from the average electronegativity of the ligand(s). Auger parameter analysis indicates that the bonding in NiO appears to have stronger contributions from initial state charge transfer from the oxygen ligands than that in the hydroxide and oxyhydroxide consistent with the considerable differences in the Ni–O bond lengths in these compounds with some relaxation of this state occurring during final state phenomena. The Auger parameter of NiOOH is, however, shifted positively, like the iodide, indicating greater polarizability of the ligands and covalency in this bonding. There is support for more direct use of relative bond lengths in interpreting differences between related compounds rather than more general electronegativity or similar parameters.

Introduction

In XPS spectra, measured core level binding energies, E_b, are commonly used to assign chemical states of elements in surfaces. The M 2p spectra of the transition metals, and Ni in particular, can contain large contributions from multiplet splitting, shake-up and plasmon loss structures. The Ni LMM Auger peak shape is also significantly influenced by multiplet splitting and shake-up structure, which can cause significant broadening.[1] The present databases (*e.g.* Phi Handbook,[1] NIST Database[2]) attempt to assign oxidation states using the Ni $2p_{3/2}$ spectrum assuming a single identifiable peak maximum and assigning the binding energy accordingly. This assumption has been shown to be invalid for many transition metal spectra,[3] *e.g.* Cr,[4] Mn,[5–8] Ni,[9,10] and Fe.[11,12] The complexity of Ni and its compounds, particularly NiO with electronic characteristics intermediate between that of a Mott–Hubbard insulator and a charge transfer semiconductor,[13] has been reviewed previously[9,14,15] and both theoretical and experimental results have been considered. Our previous works[3,9,10] have shown that the Ni $2p_{3/2}$ peak shape including shake-up and multiplet structures can be modeled with empirical peak shapes for more reliable chemical speciation analyses. Further improvement may be possible using the extra information provided by the Auger peak shape and the Auger parameter as will be indicated in this paper.

Since its conception in 1971 by Charles D. Wagner[16,17] the Auger parameter and its now common form, the modified Auger parameter (α'—known now as simply the Auger parameter), is defined as:

$$\alpha' = E_b + E_k \quad (1)$$

where E_b and E_k are the binding and kinetic energies of the (in most applications) dominant core electron and Auger electron lines for a particular element, respectively. It has been a valuable tool in the assignment of chemical states for a wide variety of surface species. In the extensive reviews by Moretti,[18,19]

[a] *Surface Science Western, The University of Western Ontario, 999 Collip Circle, London, Ontario, Canada N6G 0J3. E-mail: biesingr@uwo.ca*
[b] *Minerals and Materials Science and Technology (MMaST), Mawson Institute, University of South Australia, Mawson Lakes, South Australia 5095, Australia*
† Current address: Chengdu Green Energy and Green Manufacturing Technology R&D Center, Chengdu, Sichuan, China, 610207.

interpretation and applications of Auger parameters and Wagner plots are discussed for a wide variety of elements as free atoms, molecular species, solid surfaces, implanted and adsorbed species and metal clusters. However, in the first row transition metal series, only Ti, Cu and Zn are discussed based on the data reviewed in 1998. The NIST database[2] for the Ni Auger parameter contains 9 entries comprising Ni metal, NiO and 7 mixed oxides of Ni with V, P and Ca. Wagner's work[20,21] reports data for a number of nickel complexes in addition to the metal, oxide and fluoride. There are also other references to Auger parameter usage for Ni metal clusters (*e.g.*[22,23]), but the only other reference found to use the Ni Auger peak is the paper by Sanz and Tyuliev[24] for thin NiO films on MgO. It is appropriate therefore to extend these data and interpretation with selected nickel compounds that will assist assignment of Ni chemical states.

In a previous paper,[9] we re-examined the assignments of Ni 2p states by fitting XPS data with intra-atomic multiplet envelopes applied to $Ni(OH)_2$, NiOOH and NiO spectra. It was shown that the free ion multiplet envelopes for Ni^{2+} and Ni^{3+} effectively simulate the main line and satellite structures for $Ni(OH)_2$ and NiOOH. However, fitting the NiO Ni 2p spectral profile may involve contributions from interatomic, non-local electronic coupling and screening effects with multiplet structures significantly different from those of the free ions. The Auger parameters of these three compounds may help understand this difference particularly as it relates to initial state charge distribution and final state inter-atomic screening effects.

In XPS spectra, measured core level binding energies, E_b, involve both the ground state and the final state relaxation energies. The response of spectator electrons to the creation of a core hole and the Auger deexcitation process causes lowering of the measured binding energy as compared to the initial state binding energy and this final state relaxation energy R can vary with chemical environment. Hence, there is a need to distinguish between initial and final state contributions to the measured binding energies. It is therefore important that final state effects are correctly described if binding energy shifts are to yield useful and reliable chemical information as to the electronic structure of transition metals and their compounds. Experimentally, relaxation energy shifts are often estimated by measuring the Auger parameter shift defined by

$$\Delta\alpha' = \Delta E_b + \Delta E_k \quad (2)$$

It is usually assumed, following the derivation by Moretti,[18,19] that the relaxation energy for the doubly core-ionized state created by the Auger process equals $2R$, leading to

$$\Delta\alpha' \approx 2\Delta R \quad (3)$$

In the simplest approximation used by Wagner[21] and others,[22,23] the shifts in core level binding energy ΔE_b and in Auger transition kinetic energy ΔE_k are then:

$$\Delta E_b = -\Delta\varepsilon - \Delta R \quad (4)$$

$$\Delta E_k = \Delta\varepsilon + 3\Delta R \quad (5)$$

In this convention, positive values of $\Delta\varepsilon$, initial state contributions, and ΔR, final state contributions, result in a shift to lower binding energy. Initial state effects, $\Delta\varepsilon$, are generally understood to represent the "chemical shift" as a result of ground state electronic structure and are a function of the valence structure of the core atom, which is in turn a function of bonding to neighboring atomic valence states. Hence, in nickel compounds, these shifts are related to the electronic states (*e.g.* band structures, bond directionality) and structural parameters (*e.g.* atomic positions, Madelung constants) of the bonded atoms. To obtain this value, however, requires measurement of the Auger parameter as in eqn (1). Pan *et al.*[22] and Tao *et al.*[23] have used these initial state parameters in their work on charge transfer in Ni clusters on TiO_2 substrates. It is acknowledged that Cole *et al.*[28,30] have shown that this simple approach to analysis of the Auger parameter is not adequate for metal alloys, alkali and alkaline earths and they have developed more sophisticated methods of analysis for these systems. These methods have also been applied to transition metals and alloys[28] but not yet been applied to the nickel compounds examined here.

Following the notation used by Moretti[18,19] for transition element Wagner plots, the Auger parameter can be restated from eqn (1) as:

$$\alpha' = E_k(C'C''C''') + E_b(C) \quad (6)$$

where $E_k(C'C''C''')$ is the kinetic energy of the Auger transition involving electrons from C′, C″ and C‴ core levels and $E_b(C)$ is the binding energy of the photoelectron from core level C. In practice C′ and C are most usually the same electronic state. The specific transitions for nickel compounds are $L_3M_{45}M_{45}$ (also denoted as L_3VV, V = valence)[20,25] and Ni $2p_{3/2}$, respectively, with L_3 and $2p_{3/2}$ actually being differing notations for the same electronic state. The peak shape of the Ni metal Auger line is strongly influenced by the electron configuration and in particular by the presence of unoccupied 3d states.[26] The $^1G_4$ multiplet is likely to be the strongest component of the $L_3M_{45}M_{45}$ transition for the metal as suggested by comparison to the same transitions for Cu[27] and Zn.[20] This is not an unreasonable comparison if, on changing from the free ion state ($3d^84s^2$) to the metal, there is some transfer of the 4s electrons to the 3d orbitals. Added to this ground state electronic structure effect is local screening of the core hole which might suggest that the $L_3M_{45}M_{45}$ transition arises from a $3d^{10}$ initial state and creates a $3d^8$ final state.[28,29] Eqn (6) for Ni could then be written as:

$$\alpha' = E_k(L_3M_{45}M_{45};\ ^1G_4) + E_b(2p_{3/2}) \quad (7)$$

A specific advantage of the Auger parameter is that effects of charging and work function are cancelled out during its calculation.[18,19] Changes in α' have been shown[18,19] to be related to final state electronic relaxation occurring during photoemission processes in the central atom. There are, however, several qualifications on the measurement and interpretation of Auger parameters. Weightman[28,30] and co-workers have shown, for instance, that the relationship in eqn (3) is not valid for transition metals (particularly nickel) and their alloys.

Also implicit in eqn (3) is the assumption that $[E_b(C') - E_b(C'')]$ and $[E_b(C) - E_b(C'')]$ are constant values and are not dependent on the chemical state. Moretti[18,19] has shown this to be a

reasonable approximation for Mg, Si and Al, by examination of two different Auger parameters having different E_b(C). However, even in these cases there is some variability giving rise to standard deviations for this $\Delta\alpha'$ value of approximately 0.4 to 0.7 eV.[18,19] In addition, changes in Auger peak shapes with the chemical state and bonding may contribute to uncertainty in the position of the Auger peak used in the Auger parameter. For the case of the Ni Auger peak examined here, both $[E_b(C') - E_b(C'')]$ and $[E_b(C) - E_b(C'')]$ may be rewritten as $[E_b(2p_{3/2}) - E_b(3d_{3/2\ 5/2})]$ or $[E_b(2p_{3/2}) - E_b(3d)]$ as M_{45} actually represents multiplet combinations of the $3d_{3/2}$ and $3d_{5/2}$ valence electrons. As the d electrons are clearly involved in core–atom ligand interactions both in the ground state and during subsequent relaxation processes, as described below, variability may also arise for Ni for $[E_b(2p_{3/2}) - E_b(3d)]$.

In summary, the Auger parameter method can be used to separate the initial state, $\Delta\varepsilon$, and final state, ΔR, contributions to ΔE_b.[22,23,31,32] However, for nickel, the assumption discussed above is required for calculation of final state effects, ΔR, from eqn (3), which are in turn required for the calculation of initial state effects, $\Delta\varepsilon$. Thus variations in both ΔR and $\Delta\varepsilon$ may be due to variability in $[E_b(2p_{3/2}) - E_b(3d)]$. With these qualifications, it is useful to calculate and consider both ΔR and $\Delta\varepsilon$ for nickel metal and its compounds. These effects are examined here with spectra and peak fitting parameters from a series of quality reference samples. We examine the Auger parameters first for the metal and alloys, then the nickel halides as models for the interpretation of initial and final state and their contributions and then the Ni oxide, hydroxide and oxyhydroxide compounds.

Experimental

XPS analyses were carried out with a Kratos Axis Ultra spectrometer using a monochromatic Al Kα (15 mA, 14 kV) X-ray source. A number of samples (Ni metal, NiI_2) were also analyzed with a (non-monochromatic) Mg Kα X-ray (15 mA, 15 kV) source. The instrument work function was calibrated to give an Au $4f_{7/2}$ metallic gold binding energy of 83.95 eV. The spectrometer dispersion was adjusted to give a binding energy of 932.63 eV for metallic Cu $2p_{3/2}$. The Kratos charge neutralizer system was used for all analyses of non-conductive samples. Charge neutralization was deemed to have been fully achieved by monitoring the C 1s signal for adventitious carbon. A sharp main peak with no lower binding energy structure is generally expected. Instrument base pressure was 8×10^{-10} Torr. High-resolution spectra were obtained using an analysis area of $\sim 300 \times 700$ μm and either a 10 eV or 20 eV pass energy (20 eV was used for all Ni LMM Auger spectral results). These pass energies correspond to Ag $3d_{5/2}$ FWHM of 0.47 eV and 0.55 eV, respectively.

A single peak (Gaussian 70%—Lorentzian 30%), ascribed to alkyl type carbon (C–C, C–H), was fitted to the main peak of the C 1s spectrum for adventitious carbon. A second peak is usually added that is constrained to be 1.5 eV above the main peak, and of equal full width half maximum (FWHM) to the main peak. This higher binding energy peak is ascribed to an alcohol (C–OH) and/or ester (C–O–C) functionality. Further high binding energy components (*e.g.* C═O, 2.8–3.0 eV above the main peak; O–C═O, 3.6–4.3 eV above the main peak; CO_3^{2-}, 3.8–4.8 eV above the main peak) can also be added if required. Spectra from insulating samples have been charge corrected to give the adventitious C 1s spectral component (C–C, C–H) a binding energy of 284.8 eV. This process has an associated error of ±0.1–0.2 eV.[33] The spectra for all (argon ion sputter cleaned) metallic species are referenced to Au $4f_{7/2}$ at 83.95 eV.

Powder and polycrystalline materials were used to eliminate the possibility of photoelectron diffraction effects, which can influence splitting patterns.[34,35] They are also more representative of the majority of samples in practical analyses of air-exposed multi-component materials. Survey scan analyses for selected samples are presented in Appendix I.

Spectra were analyzed using CasaXPS software[36] (version 2.3.14). Gaussian (100–X%)—Lorentzian (X%), defined in CasaXPS as GL(X), profiles were used for each component. Individual multiplet and shake-up components as well as C 1s components and nickel compound anion species spectra have been fit with line-shapes of GL(30). For metallic and conductive species core lines, asymmetry was defined in the form of LA(α, β, m) where α and β define the spread of the tail on either side of the Lorentzian component (α and $\beta > 1$). The parameter m specifies the width of the Gaussian used to convolute the Lorentzian curve. A standard Shirley background is used for all spectra.

Powder and metal samples of highest purity readily available were purchased from Alfa Aesar. All powder samples were mounted on non-conductive adhesive tape. Metal and alloy samples were sputter cleaned using a 4 kV argon ion beam to remove all oxide and carbonaceous species. The powder samples were not sputter cleaned prior to analysis, as it is well known that this can cause reduction of oxidized species. Alloy A600 has a nominal composition of C 0.15 (wt%) max., Cr 14.0–17.0, Cu 0.50 max., Fe 6.00–10.0, Mg 1.00 max., S 0.015 max., Si 0.50 max. and Ni 72 min. Alloy A800 has a nominal composition of C 0.06–0.10, Cr 19.0–23.0, Fe 39.5 min., Al 0.15–0.60, Ti 0.15–0.60 (with a Al : Ti of 0.85–1.20) and Ni 30.0–35.0. NiO, γ-NiOOH and $Ni(OH)_2$ samples are described in ref. 9 and 10. The compounds NiF_2, $NiCl_2$, $NiBr_2$ and NiI_2 were obtained in powder form (99+ wt% purity, anhydrous) from Alfa Aesar. All four compounds were shipped under argon and introduced *via* an argon filled glove box attached to the XPS instrument. The powder samples were checked for purity by powder X-ray diffraction (XRD) using an Inel diffractometer equipped with a XRG 3000 generator and a CPS 120 curved position sensitive detector using monochromated Cu Kα radiation (λ = 1.54056 Å).

Results

There is a large body of work based on the use of XPS to examine the surfaces of nickel metal, alloys and oxides with varying methods of chemical state identification. Some of this work has been reviewed previously,[9,22,23,32] and it is clear that an understanding of multiplet splitting and satellite structure is crucial to the interpretation of the Ni 2p line-shape.[37,38] Our recent[3,9,10] work presents improved curve-fitting methods for the Ni $2p_{3/2}$ spectra that can be used to elucidate the relative

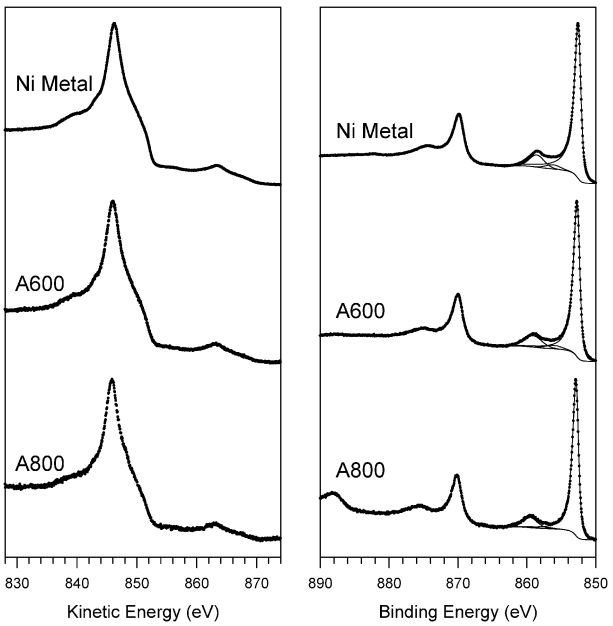

Fig. 1 Ni LMM Auger (left) and Ni 2p (right) spectra for Ni metal, Alloy A600 and Alloy A800.

concentrations of nickel compounds in a mixture. These fitting procedures have been applied to the compounds used in this study. Alloy A600 and alloy A800 spectra for Ni $2p_{3/2}$ have been fitted with an asymmetric line-shape and plasmon loss peaks as for the nickel metal (Fig. 1) and spectra for the Ni halides (Fig. 2) have been fitted using line-shapes from parameters derived from standard samples. Fits to the Ni $2p_{3/2}$ spectra of the oxide, hydroxide and oxyhydroxide have been reported previously[3,9,10] and the spectra are presented again in Fig. 3. Table 1 summarizes these results. Fig. 1–3 also present the LMM Auger peak shapes for the metal and alloys, halides, and oxide, hydroxide and oxyhydroxide, respectively. Anion binding energies for the halides with FWHM at 10 and 20 eV pass energies are reported in Table 2.

Auger parameters calculated using the peak maxima for both the Ni $2p_{3/2}$ and $L_3M_{45}M_{45}$ Auger structures (charge corrected when necessary to C 1s at 284.8 eV) along with the calculated Auger parameter values are presented in Table 3. For these values, it is assumed that the position of the Auger peak maximum is not significantly altered by changes in the peak shape. The Wagner plots for the oxides referenced to the metal and alloys (Fig. 4) and halides (Fig. 5) are also presented. In the Wagner plot for Ni of $E_k(L_3M_{45}M_{45})$ values (y axis) *versus* $E_b(2p_{3/2})$ values (x axis, smaller values run to the right) constant α' values are represented with lines of slopes of -1 (eqn (6)). Species with greater ΔR relaxation values, generally of greater covalency, are represented in the upper part of the plot with more ionic species with smaller α' values in the lower part. Covalency has also been shown to correlate with the 2p–3d exchange interaction (*via* a scaling factor), with a larger exchange interaction (*i.e.* more covalency) leading to more splitting, corresponding to wider overall Auger peak widths.[39] Table 3 sets out the calculation of the initial and final state shifts for each nickel compound referenced to the nickel metal according to eqn (4) and (5). The assumptions made in this calculation are that eqn (3) applies and that the $L_3M_{45}M_{45}$ Auger peak position is not significantly altered by peak shape changes between the different nickel containing compounds. Both these assumptions will be examined in the discussion.

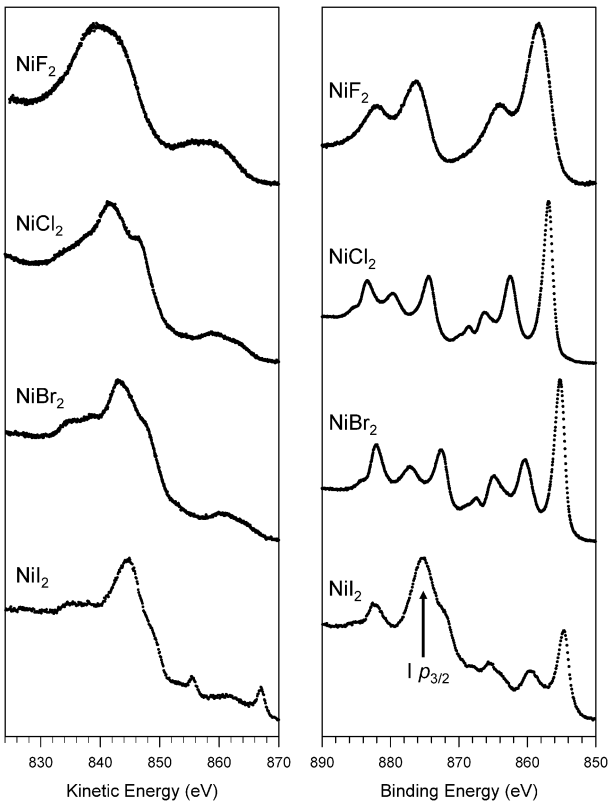

Fig. 2 Ni LMM Auger (left) and Ni 2p (right) spectra for NiF_2, $NiCl_2$, $NiBr_2$ and NiI_2. Note the overlap of I $3p_{3/2}$ peak with the Ni 2p spectrum for NiI_2.

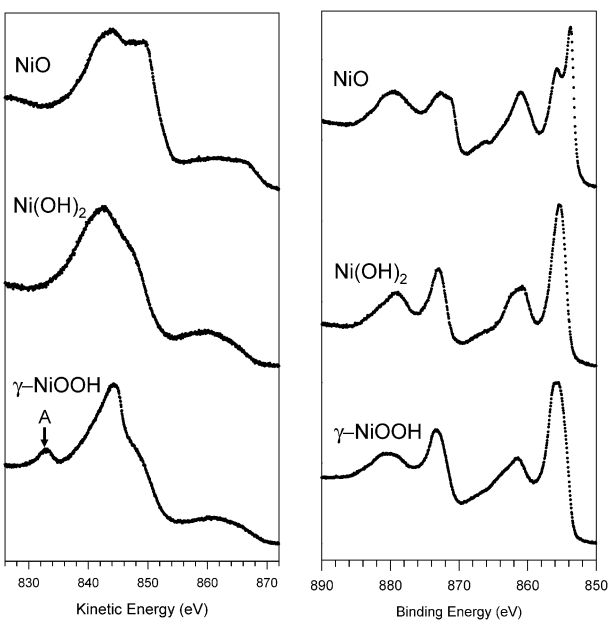

Fig. 3 Ni LMM Auger spectra (left) and Ni 2p (right) spectra for NiO, $Ni(OH)_2$ and NiOOH.

Table 1 Ni $2p_{3/2}$ spectral fitting parameters: binding energy (eV), percentage of total area, FWHM value (eV) for each pass energy, and spectral component separation (eV)

Compound	Peak 1 (eV)[a]	%	Peak 1, FWHM, 10 eV pass energy	Peak 1, FWHM, 20 eV pass energy	Peak 2 (eV)	Δ peak 2 − peak 1 (eV)[a]	%	Peak 2, FWHM, 10 eV pass energy	Peak 2, FWHM, 20 eV pass energy	Peak 3 (eV)	Δ peak 3 − peak 2 (eV)	%	Peak 3, FWHM, 10 eV pass energy	Peak 3, FWHM, 20 eV pass energy	Peak 4 (eV)	Δ peak 4 − peak 3 (eV)	%	Peak 4, FWHM, 10 eV pass energy	Peak 4, FWHM, 20 eV pass energy
A600[b]	852.7	83.5		0.91	856.1	3.39		3.6		2.92	859.1	3.02		12.9		2.92				
A800[b]	852.9	85.5		0.85	856.9	4.07		2.2		2.71	859.5	2.60		12.3		2.71				
NiF_2[c]	858.1	63.5	3.62	3.75	863.6	5.48		36.6	4.85	5.54										
$NiCl_2$	856.8	43.1	1.47	1.55	858.2	1.45		7.7	1.47	1.55	859.8	1.63		2.7	1.47	1.55	862.3	2.48	27.9	2.12	2.15
$NiBr_2$	855.2	43.0	1.25	1.45	856.5	1.23		8.1	1.25	1.45	857.8	1.34		1.8	1.25	1.45	860.4	2.56	25.8	2.29	2.30

Compound	Peak 5 (eV)	Δ peak 5 − peak 4 (eV)	%	Peak 5, FWHM, 10 eV pass energy	Peak 5, FWHM, 20 eV pass energy	Peak 6 (eV)	Δ peak 6 − peak 5 (eV)	%	Peak 6, FWHM, 10 eV pass energy	Peak 6, FWHM, 20 eV pass energy	Peak 7 (eV)	Δ peak 7 − peak 6 (eV)	%	Peak 7, FWHM, 10 eV pass energy	Peak 7, FWHM, 20 eV pass energy	Peak 8 (eV)	Δ peak 8 − peak 7 (eV)	%	Peak 8, FWHM, 10 eV pass energy	Peak 8, FWHM, 20 eV pass energy
A600																				
A800																				
NiF_2																				
$NiCl_2$	865.0	2.72	8.7	2.45	2.47	866.3	1.29	5.8	1.45	1.56	868.4	2.10	3.1	1.12	1.19	869.7	1.31	1.0	0.99	1.12
$NiBr_2$	863.7	3.37	11.1	2.49	2.57	865.2	1.44	7.2	1.36	1.46	867.5	2.35	2.0	0.92	0.91	868.7	1.14	1.1	0.98	1.29

[a] Binding energies are significant to 0.1 eV but an additional figure is added because energy splittings are much more accurate than the absolute binding energies. [b] Peak 1 has an asymmetric line-shape defined in CasaXPS by LA(1.1,2.2,10). [c] Charge referenced to F 1s set to 685.23 eV.

Table 2 Binding energy and FWHM values (eV) for nickel halide anions

Compound	Element/peak	Binding energy/eV	FWHM (10 eV pass energy)	FWHM (20 eV pass energy)
NiF_2	F 1s	685.2	2.35	2.87
$NiCl_2$	Cl $2p_{3/2}$	199.9	1.07	1.14
$NiBr_2$	Br $3d_{5/2}$	69.2	0.87	0.95
NiI_2[a]	I $3d_{5/2}$	619.5	1.02	1.35

[a] Taken with Mg K(alpha) source.

Discussion

In a seminal paper,[13] Zaanen *et al.* classified transition metal compounds on the basis of their electronic structures and band gaps in a theoretical phase diagram based on values of U, from d–d Coulomb and exchange interactions, and Δ, from charge transfer of the $d^n \rightarrow d^{n+1}L$ type where L is a ligand hole. They identify regions in the phase diagram for d-band metals, Mott–Hubbard insulators, where the band gap is proportional to U, and charge transfer semiconductors, where the band gap is proportional to Δ and the electronegativity of the anion. In this classification, $NiCl_2$, $NiBr_2$ and NiI_2 are charge transfer semiconductors while NiO and NiF_2 fall into the intermediate region between Mott–Hubbard insulators and charge transfer semiconductors. The implication of this intermediate region is that both holes and electrons move primarily in d-bands. Both the electronegativity and bonding of the ligands will also be considered below. For reference, band gap,[10,40,41] Δ,[42] and anion electronegativity[43] values in eV are as follows: NiF_2 (9, 7, 3.98); $NiCl_2$ (4.7, 3.6, 3.16); $NiBr_2$ (3.5, 2.6, 2.96); NiI_2 (1.8, 1.5, 2.66); and NiO (3.6, 4.6, 3.44). The band gap[10] and anion electronegativity for $Ni(OH)_2$ are 2.78 and 3.03 (group electronegativity).

Nickel metal and alloys

Fig. 1 shows the Ni 2p and LMM Auger spectra for the metal and the two alloys. All Ni $2p_{3/2}$ spectra show asymmetric main peaks and plasmon loss structure typical of metallic nickel. Our previous work[9] has shown that the positions of the surface and bulk plasmons are at +3.7 and +6.0 eV, respectively, above the main peak for metallic Ni. It should be noted that the 6 eV satellite had been previously assigned (*e.g.* ref. 44) as a two hole $c3d^94s^2$ (c is a core hole) final state effect. The positions and intensities of the surface and bulk plasmons vary slightly for the alloys which may indicate small changes in the electronic configuration but the data on initial and final state shifts in Table 3 are within experimental error and are not sufficiently reliable to support this contention. They are also essentially indistinguishable in the Wagner plots (Fig. 4) although slight narrowing of the Auger spectra occurs from the metal to A600 and again to A800, corresponding to a narrower Auger peak width as the Ni content decreases in the alloy. This trend has also been noted for Ni–Zn alloys.[26]

The inability to separate metallic species in the Wagner plot is in accord with the series of papers by Cole *et al.*,[28,30] in which the excited atom approach is used to investigate core hole relaxation energies R in noble and transition metal alloys. It was found that relaxation shifts ΔR are determined predominantly by changes in the d electron population and are insensitive to interatomic charge transfer. Although the Auger parameter gives a correct

Table 3 Ni $2p_{3/2}$ and Ni LMM peak maximum positions, Auger parameter (α'), ΔE_b, ΔE_k, $\Delta\alpha'$, ΔR and $\Delta\varepsilon$ values

Compound	Ni $2p_{3/2}$ peak maximum E_b/eV	Ni LMM Auger peak maximum E_k/eV	Auger parameter (α')/eV	ΔE_b (Ni $2p_{3/2}$)	ΔE_k (Ni LMM)	$\Delta\alpha'$	ΔR	$\Delta\varepsilon$
Ni metal	852.54	846.22	1698.76					
A600	852.70	846.02	1698.72	0.16	−0.20	−0.04	−0.02	−0.14
A800	852.85	845.87	1698.72	0.31	−0.35	−0.04	−0.02	−0.29
NiO	853.78	843.93	1697.71	1.24	−2.29	−1.05	−0.53	−0.71
$Ni(OH)_2$	855.80	842.58	1698.38	3.26	−3.64	−0.38	−0.19	−3.07
γ-NiOOH[a]	855.75	844.29	1700.04	3.21	−1.93	1.28	0.64	−3.85
NiF_2[b]	858.12	839.74	1697.86	5.58	−6.48	−0.90	−0.45	−5.13
$NiCl_2$	856.77	841.88	1698.65	4.23	−4.34	−0.11	−0.06	−4.17
$NiBr_2$	855.27	843.25	1698.52	2.73	−2.97	−0.24	−0.12	−2.61
NiI_2	854.46	845.23	1699.69	1.92	−0.99	0.93	0.46	−2.38

[a] Ni LMM Auger has a unique peak shape with an extra high binding energy peak. [b] Charge referenced to F 1s set to 685.23 eV.

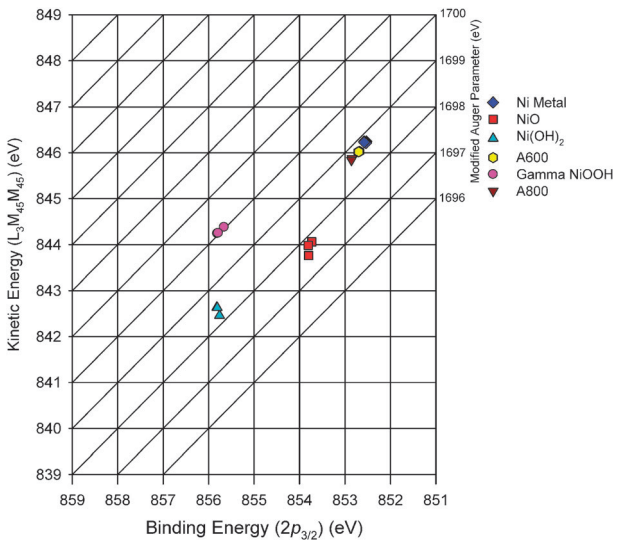

Fig. 4 Ni $2p_{3/2}$–Ni LMM Wagner plot for Ni metal, Ni alloys, NiO, $Ni(OH)_2$ and NiOOH.

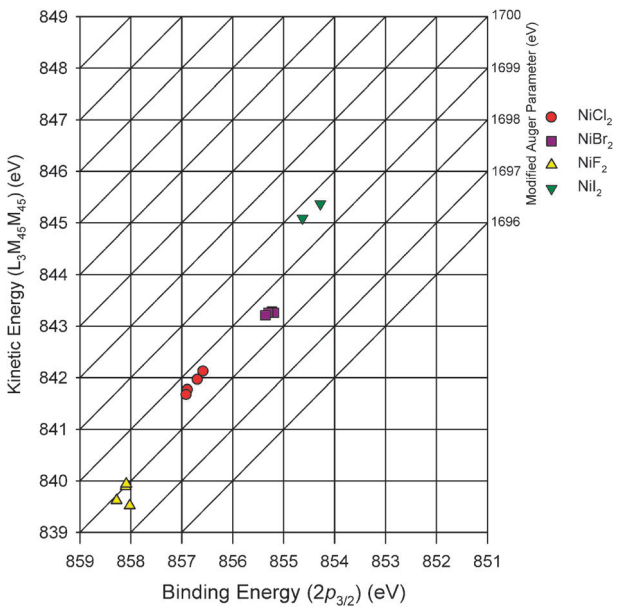

Fig. 5 Ni $2p_{3/2}$–Ni LMM Wagner plot for Ni halides.

indication of the sign of relaxation energy shifts, the approximation $\Delta R \approx \Delta\alpha/2$ does not provide a reliable estimate of their magnitude and, in the case of transition metal and alloys ($p > 2$), $\Delta\alpha/2$ overestimates ΔR. Thus, it is not a useful indication of relaxation shifts in the metal and alloys.

Nickel halides

Fig. 2 shows the succession of nickel halide Ni 2p and LMM Auger spectra. The Ni $2p_{3/2}$ peak increases in binding energy from the iodide through to the fluoride, normally taken to indicate increasing positive charge on the core nickel ion. This is supported by the strong relationship between Ni $2p_{3/2}$ binding energy and electronegativity of the ligand as suggested in our earlier paper (ref. 9, see Fig. 8).

The chloride and bromide show similar Ni 2p peak structures. Subtraction of the overlap of the I $3p_{3/2}$ peak from the Ni 2p peak structure gives a similar structure to the chloride and bromide for the Ni $2p_{3/2}$. The degree of covalency for these compounds has been calculated to be $NiI_2 > NiBr_2 > NiCl_2$.[45] This progressive change in bonding is reflected in the halide LMM spectra which show progressive changes from the chloride to the iodide. Specifically, the higher kinetic energy shoulder on the main peak diminishes from the chloride to the iodide. The overall Auger peak width also decreases from the chloride to the iodide and is correlated with a reduction in effective d-hole concentration.[26,39] The fluoride does not fit into this trend with a peak width between chloride and bromide.

Also in contrast to the other three halides, the fluoride shows only two Ni $2p_{3/2}$ peaks, a broad main peak and a smaller, broad satellite peak. The nickel in the fluoride structure has a slightly distorted octahedral coordination (Ni–X of 2.005 Å × 4; 2.007 Å × 2[46]) as compared to the regular octahedral coordination for the Ni chloride, bromide and iodide (Ni–X of 2.428 Å, 2.58537 Å, 2.78652 Å, respectively[47]). This is reflected by a change in crystal structure between the nickel fluoride (space group $P4_2/mnm$, rutile-like structure) and other nickel halides ($R3m$, $CdCl_2$ like structure) which may contribute to this different spectral profile. It is possible that this octahedral distortion contributes to the width of the broadened Ni $2p_{3/2}$ peaks with broadening also observed for the fluoride LMM Auger peak. NiF_2 is reported to have a band gap of ~9 eV[41] which, with the large electronegativity of the anion (*i.e.* 3.98),[43] makes it unlikely to fit easily into the criteria

specified for charge transfer semiconductors. These differences from the other halides are also in accord with the Zaanen *et al.*[13] classification for NiF_2 as intermediate between Mott–Hubbard insulators and charge transfer semiconductors.

The shifts in binding energy of the halides as a function of electronegativity of the anion (ref. 9, Fig. 8) are strongly correlated but not linear with the fluoride and chloride deviating to higher binding energy and the iodide to lower binding energy. The correlation coefficient for linear interpolation between the Ni $2p_{3/2}$ binding energies and electronegativity values is 0.89, whereas the correlation between the binding energy values and Ni–X distance is 0.95, indicating that geometrical consideration (which by default takes into account electronegativity as well as ionic radius and bonding) may be a better indicator of binding energy for closely related compounds.

Analysis of the initial and final state effects for the halides (Table 3) shows that their binding and kinetic energy shifts are dominated by the initial ground electronic state effects, $\Delta\varepsilon$, which are much larger (-5.15 to -2.45 eV) than the final state shifts, ΔR (-0.45 to $+0.45$ eV). These initial state effects induce a shift to higher binding energy, as in eqn (4). The initial state effect decreases in magnitude from fluoride to iodide suggesting a progressively decreasing positive ground state valence state. The correlation of $\Delta\varepsilon$ with Na–X distance (or electronegativity) is poorer as compared to the same correlations with binding energy possibly suggesting that the assumption of $\Delta\alpha \approx 2\Delta R$ and/or that $[E_b(2p_{3/2}) - E_b(3d)]$ is constant is not entirely valid and that this is affected by a local chemical environment.

The final state effects ΔR due to the polarizability of the larger halide ions, particularly the diffuse iodide ion, are seen in the positive ΔR relaxation shift to lower binding energy offsetting the $-\Delta\varepsilon$ shift to higher binding energy. These changes are reflected in the Wagner plot (Fig. 5) where the Auger parameter position of the iodide shows greater covalency and the fluoride greater ionicity together with the shifts in apparent valency reflected in the binding energies. The same reduction of correlation of ΔR, as compared to Ni $2p_{3/2}$ binding energy, with either electronegativity or Na–X distance is observed as for $\Delta\varepsilon$. This is most probably due to the nature of the calculation of $\Delta\varepsilon$ and ΔR such that any breakdown in the assumption of eqn (3) or that $[E_b(2p_{3/2}) - E_b(3d)]$ is constant is propagated through the calculation of ΔR to $\Delta\varepsilon$ such that where ΔR is shifted to positive binding energy, $\Delta\varepsilon$ will be shifted commensurately negatively.

Nickel oxide, hydroxide and oxyhydroxide

Fig. 3 for the Auger spectrum of NiO shows a well resolved two peak structure while in the $Ni(OH)_2$ spectrum the two peaks are much broader. The Ni(III) compound γ-NiOOH gives rise to a unique peak shape with a characteristic lower kinetic energy peak at 832.8 eV. The Auger parameters for these oxides, combining the previously fit Ni $2p_{3/2}$ XPS and Auger spectra, are listed in Table 3. NiO is isostructural to rock salt with Ni having regular octahedral coordination and a Ni–O distance of 1.81 Å (unit cell 4.18 Å) whereas $Ni(OH)_2$ is isostructural with portlandite ($Ca(OH)_2$) with space group $P\bar{3}m1$ and Ni–O (also in regular octahedral coordination) distance of 2.08 Å. There remains some uncertainty about the exact crystallography of γ-NiOOH, particularly in terms of stacking faults, however there does seem to be agreement that it consists of Ni-containing layers that are essentially the same as for β-NiOOH with intercalated H_2O, H^+ and/or alkali cations.[48] β-NiOOH displays distorted octahedral coordination to O with four short bonds of 1.87 Å and two longer bonds of 2.03 Å,[49] possibly giving rise to the distinctly different Auger peak shape.[50] A correlation between the overall Auger peak width and effective d hole concentration[26] is again observed with NiO having a slightly narrower peak width than $Ni(OH)_2$. γ-NiOOH (*i.e.* Ni(III)) has the broadest peak width of all the compounds studied.

Analysis of the initial and final state effects in these oxides (Table 3) shows that the initial state shift for NiO (-0.7 eV) is much smaller than those for $Ni(OH)_2$ (-3.1 eV) or NiOOH (-3.8 eV). The final state effect for NiO (-0.53 eV) represents a much larger shift to higher binding energy than that for $Ni(OH)_2$ (-0.19 eV) with that of NiOOH ($+0.64$ eV) shifting to lower binding energy. The effective valence or oxidation state of the Ni in NiO is much smaller than that expected from an analysis of ligand electronegativities. The plot of binding energy *versus* average electronegativity of the ligand (ref. 9, Fig. 8) would indicate that a Ni $2p_{3/2}$ binding energy for NiO near 856.5 eV might have been expected rather than 854.7 eV (peak centre of gravity value) reported previously[9] or the 853.8 eV (peak maximum) found in the improved fit reported in this paper. It appears that considerable electron sharing (or covalency) between the Ni and surrounding O is occurring in the ground electronic state which manifests as reduced apparent oxidation and a smaller relative initial state shift.

This proposal is similar in concept, but not as complete in terms of electron transfer, as the $\underline{c}d^9\underline{L}$ (where $\underline{c}$ refers to a core electron hole and $\underline{L}$ is a ligand hole) charge transfer configuration previously invoked[44,51] to explain the relatively low binding energy of the main Ni $2p_{3/2}$ peak. However, in the ground state no $\underline{c}$ is present and the initial state electron configuration is better written as $d^{8+\delta}\underline{L}^{-\delta}$. This interpretation is in agreement with quantum chemical calculations on NiO using a variety of approaches which consistently suggest a Ni ground state charge of less than 2, with the charge resulting from the more reliable density functional and hybrid density functional Hartree–Fock approaches ranging from 1.68 to 1.33.[52]

Further strength is added to this proposition by the very small Ni–O bond length in NiO which suggests a high degree of orbital overlap. In contrast, the bond lengths are considerably longer and the corresponding initial state shifts larger for the hydroxide and oxyhydroxide implying that the initial ground state bonding is less covalent and less electron sharing between the Ni and surrounding ligands is occurring. In these compounds, the measured binding energies are consistent with the electronegativity of the anions as expected for the Zaanen *et al.*[13] charge transfer semiconductor classification. This proposal is also consistent with the, also surprisingly low, O 1s binding energy for NiO which is the smallest of all O 1s binding energies reported in ref. 10 at 529.30 eV, as compared to a range of oxide and hydroxide species of Cr, Mn, Fe, Co and Ni. This binding energy suggests that the shared Ni–O electrons are polarized back towards the O resulting in the very low measured binding energy.

In final state effects, the negative shift in the Auger parameter of NiO as compared to that of the metal is larger than that of the hydroxide, oxyhydroxide and even the fluoride. This may imply

that the charge transfer from the O 2p band is mainly reflected in the initial state for NiO with further, but more minor, transfer in the final state effects to form $\underline{c}d^9\underline{L}$. In support of the $\underline{c}d^9\underline{L}$ explanation the multiple cluster quantum chemical simulation of Ni 2p XPS line shapes for NiO by van Veenendaal and Sawatsky[53] indicates that interactions of the central Ni atom (core hole $\underline{c}$) with neighboring NiO_6 octahedra result in broadening of the main line and the satellite and the lowest binding energy final state had predominant $\underline{c}d^9\underline{L}$ character with charge transfer from the adjacent O atoms. It is also noted that the O 2p band is overlapped with the Ni 3d band in NiO UV photoemission.[54]

This explanation would agree with the observation[9] that the NiO multiplet and satellite envelopes in Ni 2p spectra from NiO cannot be fit with the free ion Gupta and Sen components[55,56] of Ni^{2+}. Conversely, the $Ni(OH)_2$ and NiOOH multiplet and satellite envelopes are reasonably fit by the free ion Ni^{2+} and Ni^{3+} Gupta and Sen parameters, respectively, suggesting that local inter-atomic contributions are not dominant in these cases. The Auger parameter of NiOOH is, however, shifted positively like the iodide indicating higher covalency in the bonding during final state processes.

In summary, the Auger parameter analysis of the oxides has again indicated that the bonding in NiO appears to have stronger contributions from charge transfer from the oxygen ligands than that in the hydroxide and oxyhydroxide as reflected in the relative initial state shifts. As discussed in our previous paper,[9] the reasons for the differences in the ligand transfer between the oxide and the hydroxide or oxyhydroxide may only be resolved by further theoretical modelling of the NiO structure using all inter-atomic wave function mixing and coupling/re-coupling angular momentum contributions.

Conclusions

The critical role of the Auger parameter in providing insight into both the initial state chemical shift and the final state factors affecting the measured XPS binding energies is clearly illustrated in these results. There is also support for more direct use of relative bond lengths in interpreting differences between related compounds rather than more general electronegativity or similar parameters. There are significant qualifications as to the analysis of the initial and final state shifts, particularly in the assumption of $\Delta\alpha \approx 2\Delta R$, but consideration of these values together with the structural and electronic factors has provided further insight into the differences between the nickel compounds examined.

The metal and the two alloys are essentially indistinguishable in the Wagner plots and in initial and final states although the positions and strengths of the surface and bulk plasmons vary slightly for the alloys which may indicate small changes in the electronic configuration. A narrowing of overall Auger peak width is observed as the Ni content decreases in the alloy as compared to the metal.

Analysis of the initial and final state effects in the halides shows that their binding and kinetic energy values are dominated by the initial state effects, $\Delta\varepsilon$, which are much larger than the final state shifts, ΔR. The Ni $2p_{3/2}$ peak increases in binding energy from the iodide through to the fluoride showing the increasing positive charge on the core nickel ion in the initial state induced by increasing electronegativity of the ligands. The degree of covalency, $NiI_2 > NiBr_2 > NiCl_2$,[45] is reflected in the Wagner plot where the more polarizable iodide and bromide have greater ΔR and α'. Correction of the measured binding energy by the final state ΔR to give the initial states is relatively small in the nickel halides. The overall Auger peak width also decreases from the chloride to the iodide and is correlated with a reduction in effective d-hole concentration.

Analysis of the initial and final state effects for nickel oxide, hydroxide and oxyhydroxide shows that the initial state shift for NiO is much smaller than those of $Ni(OH)_2$ or NiOOH. The effective valence or oxidation state is also much smaller than that inferred from the plot against average electronegativity of the ligand. In NiO, it appears that partial electron charge transfer from the 2p ligand band to the Ni 3d orbitals has occurred to a greater extent in the initial, rather than final state. This is reflected in the small initial state shift with an apparent transfer of charge to form a $d^{8+\delta}L^{-\delta}$ initial state and some relaxation of this state occurring during final state phenomena to form $\underline{c}d^9\underline{L}$. There is support for the $\underline{c}d^9\underline{L}$ mechanism in both theoretical and UV photoemission studies. The reasons for the differences between NiO and the hydroxide and oxyhydroxide in the initial state charge transfer remain unclear but are likely to be related to the relatively short Ni–O bond length in NiO. Also the $Ni(OH)_2$ and NiOOH multiplet and satellite envelopes are reasonably fit by the free ion Ni^{2+} and Ni^{3+} parameters, respectively, suggesting that local inter-atomic contributions are not dominant in these cases. The Auger parameter of NiOOH is, however, shifted positively like the iodide indicating higher polarizability of the ligands and covalency in the bonding during final state phenomena. NiOOH, with the highest effective d-hole, has the broadest Auger peak width.

Appendix I

Table A1.

Table A1 Results from selected XPS survey scan analyses in atomic percent

Compound	C	N	O	F	Na	Mg	Si	S	P	Cl	Ca	Fe	Cr	Ni	Br	Mo	I	Bi
A600	4.6		2.9									5.6[a]	15.5	71.4				
A800	4.7		2.5									47.1	18.7	27.1				
NiF_2	6.2		5.2	53.0										35.5				
$NiCl_2$	5.1		2.5							57.3				35.1				
$NiBr_2$	13.4		1.8											31.8	53.0			
NiI_2	15.6		1.2	1.8										22.0[b]			59.4	

[a] Underestimate of the Fe amount due to Fe 2p overlap with Ni Auger peak structure. [b] Underestimate of the Ni amount due to slight Ni $2p_{3/2}$ overlap with the I $3p_{3/2}$ peak.

Acknowledgements

The paper has been considerably improved by valuable comments and references from the reviewers. The Kratos Axis Ultra was funded in part by a Canadian Foundation for Innovation (CFI) grant. The work was partly funded by a scholarship (MCB) from the Applied Centre for Structural and Synchrotron Studies (now MMaST) at UniSA. A travel grant to MCB from Surface Science Western is also gratefully acknowledged.

References

1 J. F. Moulder, W. F. Stickle, P. E. Sobol and K. D. Bomben, *Handbook of X-ray Photoelectron Spectroscopy*, Perkin-Elmer Corp., Eden Prairie, MN, 1992.
2 C. D. Wagner, A. V. Naumkin, A. Kraut-Vass, J. W. Allison, C. J. Powell and J. R. Rumble, Jr., *NIST Standard Reference Database 20, Version 3.4*, (web version) (http:/srdata.nist.gov/xps/), 2003.
3 M. C. Biesinger, B. P. Payne, A. P. Grosvenor, L. W. M. Lau, A. R. Gerson and R. St. C. Smart, *Appl. Surf. Sci.*, 2011, **257**, 2717.
4 M. C. Biesinger, C. Brown, J. R. Mycroft, R. D. Davidson and N. S. McIntyre, *Surf. Interface Anal.*, 2004, **36**, 1550.
5 H. W. Nesbitt and D. Banerjee, *Am. Mineral.*, 1998, **83**, 305.
6 D. Banerjee and H. W. Nesbitt, *Geochim. Cosmochim. Acta*, 1999, **63**, 3025.
7 D. Banerjee and H. W. Nesbitt, *Geochim. Cosmochim. Acta*, 1999, **63**, 1671.
8 D. Banerjee and H. W. Nesbitt, *Geochim. Cosmochim. Acta*, 2001, **65**, 1703.
9 A. P. Grosvenor, M. C. Biesinger, R. St. C. Smart and N. S. McIntyre, *Surf. Sci.*, 2006, **600**, 1771.
10 M. C. Biesinger, B. P. Payne, L. W. M. Lau, A. R. Gerson and R. St. C. Smart, *Surf. Interface Anal.*, 2008, **41**, 324.
11 N. S. McIntyre and D. G. Zetaruk, *Anal. Chem.*, 1977, **49**, 1521.
12 A. P. Grosvenor, B. A. Kobe, M. C. Biesinger and N. S. McIntyre, *Surf. Interface Anal.*, 2004, **36**, 1564.
13 J. Zaanen, G. A. Sawatzky and J. W. Allen, *Phys. Rev. Lett.*, 1985, **55**, 418.
14 H. A. E. Hagelin-Weaver, J. F. Weaver, G. B. Hoflund and B. G. N. Salaita, *J. Electron Spectrosc. Relat. Phenom.*, 2004, **134**, 139.
15 H. A. E. Hagelin-Weaver, J. F. Weaver, G. B. Hoflund and B. G. N. Salaita, *J. Alloys Compd.*, 2005, **389**, 34.
16 C. D. Wagner, in *Proceedings of the International Conference Held at Asilomar*, ed. D. A. Shirley, Pacific Grove, CA, USA, North-Holland, Amsterdam, 7–10 September, 1971, 1972, p. 861.
17 C. D. Wagner, *Anal. Chem.*, 1972, **44**, 967.
18 G. Moretti, *J. Electron Spectrosc. Relat. Phenom.*, 1998, **95**, 95.
19 G. Moretti, in *Surface Analysis by Auger and X-ray Photoelectron Spectroscopy*, ed. D. Briggs and J. T. Grant, IM Publications, Chichester, UK, 2003, p. 501.
20 C. D. Wagner, L. H. Gale and R. H. Raymond, *Anal. Chem.*, 1979, **51**, 466.
21 C. D. Wagner and J. A. Taylor, *J. Electron Spectrosc. Relat. Phenom.*, 1982, **28**, 211.
22 J. S. Pan, J. G. Tao, C. H. A. Huan, Z. Zhang, J. W. Chai and S. J. Wang, *Appl. Surf. Sci.*, 2010, **256**, 4850.
23 J. G. Tao, J. S. Pan, C. H. A. Huan, Z. Zhang, J. W. Chai and S. J. Wang, *Surf. Sci.*, 2008, **602**, 2769.
24 J. M. Sanz and G. T. Tyuliev, *Surf. Sci.*, 1996, **367**, 196.
25 G. C. Allen, P. M. Tucker and R. K. Wild, *Surf. Sci.*, 1977, **68**, 469.
26 P. T. Andrews, T. Collins and P. Weightman, *J. Phys. C: Solid State Phys.*, 1981, **14**, L957.
27 E. D. Roberts, P. Weightman and C. E. Johnson, *J. Phys. C: Solid State Phys.*, 1975, **8**, L301.
28 R. J. Cole, P. Weightman and J. A. D. Matthew, *J. Electron Spectrosc. Relat. Phenom.*, 2003, **133**, 47.
29 N. Mårtensson, P. Hedegård and B. Johansson, *Phys. Scr.*, 1984, **29**, 154.
30 R. J. Cole, N. J. Brooks, P. Weightman and J. A. D. Matthew, *Phys. Rev. B: Condens. Matter*, 1995, **15**, 2976.
31 B. Richter, H. Kuhlenbeck, H. J. Freund and P. S. Bagus, *Phys. Rev. Lett.*, 2004, **93**, 026805.
32 P. S. Bagus, A. Wieckowski and H. Freund, *Chem. Phys. Lett.*, 2006, **420**, 42.
33 D. J. Miller, M. C. Biesinger and N. S. McIntyre, *Surf. Interface Anal.*, 2002, **33**, 299.
34 D. Briggs and J. C. Rivière, in *Practical Surface Analysis by Auger and X-ray Photoelectron Spectroscopy*, ed. D. Briggs and M. P. Seah, John Wiley & Sons, Chichester, UK, 1983, p. 135.
35 P. A. W. Van der Heide, *J. Electron Spectrosc. Relat. Phenom.*, 2008, **164**, 8.
36 N. Fairley, http://www.casaxps.com, © Casa software Ltd. 2005.
37 M. W. Roberts and R. St. C. Smart, *J. Chem. Soc., Faraday Trans.*, 1984, **80**, 2957.
38 N. S. McIntyre, D. G. Zetaruk and D. Owen, *Appl. Surf. Sci.*, 1978, **2**, 55.
39 G. van der Laan, B. T. Thole, G. A. Sawatzky and M. Verdaguer, *Phys. Rev. B: Condens. Matter*, 1988, **37**, 6587.
40 C. R. Ronda, G. J. Arends and C. Hass, *Phys. Rev. B: Condens. Matter*, 1987, **35**, 4038.
41 A. S. Barrière, J. Pichon, S. Lotfi and G. Gevers, *Thin Solid Films*, 1982, **89**, 77.
42 G. van der Laan, J. Zaanen, G. A. Sawatzky, R. Karnatak and J.-M. Esteva, *Solid State Commun.*, 1985, **56**, 673.
43 A. L. Allred, *J. Inorg. Nucl. Chem.*, 1961, **17**, 215.
44 S. Hufner, *Photoelectron spectroscopy, Solid State Science Series*, Springer-Verlag, vol. 82, 1995, (chapter 3 and references therein).
45 M. G. Brik, *Phys. B (Amsterdam, Neth.)*, 2007, **387**, 69.
46 J. C. Taylor and P. W. Wilson, *Acta Crystallogr.*, 1974, **B30**, 554.
47 M. G. Brika, N. M. Avram and C. N. Avram, *Physica B (Amsterdam)*, 2006, **371**, 43.
48 L. Eriksson, U. Palmqvist, H. Rundlöf, U. Thuresson and R. Sjövall, *J. Power Sources*, 2002, **107**, 34.
49 A. Demourgues, L. Gautier, A. V. Chadwick and C. Delmas, *Nucl. Instrum. Methods Phys. Res., Sect. B*, 1977, **133**, 39.
50 P. Oliva, J. Leonardi, J. F. Laurent, C. Delmas, J. J. Braconner, M. Figlarz, F. Fievet and A. de Guibert, *J. Power Sources*, 1982, **8**, 229.
51 A. F. Carley, S. D. Jackson, J. N. O'Shea and M. W. Roberts, *Surf. Sci.*, 1999, **440**, L868.
52 T. Bredow and A. R. Gerson, *Phys. Rev. B: Condens. Matter*, 2000, **61**, 5194.
53 M. A. van Veenendaal and G. A. Sawatsky, *Phys. Rev. Lett.*, 1993, **70**, 2459.
54 P. S. Bagus, R. Broer, W. A. de Jong, W. C. Nieuwpoort, F. Parmiginai and L. Sangaletti, *Phys. Rev. Lett.*, 2000, **84**, 2259.
55 R. P. Gupta and S. K. Sen, *Phys. Rev. B: Condens. Matter*, 1974, **10**, 71.
56 R. P. Gupta and S. K. Sen, *Phys. Rev. B: Condens. Matter*, 1975, **12**, 15.

